Journal of the Brazilian Society of Mechanical Sciences and Engineering (2018) 40:545
https://doi.org/10.1007/s40430-018-1465-1

TECHNICAL PAPER

Turbulent impingement jet heat transfer on concave surfaces for aeronautical applications

Saulo A. G. Salcedo[1] · Adaiana F. Gomes da Silva[1] · Cláudia R. Andrade[1]

Received: 9 April 2018 / Accepted: 19 October 2018 / Published online: 28 October 2018

Abstract

Turbulent impingement jet heat transfer on concave surfaces has been employed in different engineering applications, e.g., aviation industry. In the aircraft anti-icing systems, hot air from the engine compressor impinges on the inside surface of the leading edge through small drilled holes, configuring the so-called piccolo tube system. A critical aspect in the design of such system is the prediction of heat transfer impinging jets from the piccolo tube. The correct evaluation of the heat transfer rate in such devices is of great interest to optimize both the anti-icing performance and the hot-air bleeding from the high-pressure compressor. Therefore, the present study develops a parametric study of the impingement jet flow on concave surfaces employing the CFD tool. The main goal is to determine the effect of the jet Mach number on this heat transfer mechanism. The present results also showed that at lower *H*/*d* conditions, i.e., lower jet-to-impinging surface distances, the temperature field exhibits a more efficient heating process inside the domain, resulting in greater Nusselt number values. A correlation taking into account geometric parameters such as the jet-to-jet spacing and the jet-to-impinging surface distance and jet Mach number is also proposed.

Keywords Hot-air anti-icing system · Heat transfer · Turbulent impingement jet · Mach number

List of symbols

c	Sound velocity
d	Jet diameter
H	Jet-to-impinging surface distance
$h(x,y)$	Local convection heat coefficient
h_{ave}	Average convection heat coefficient
k	Air thermal conductivity
Ma	Mach number = V/c
$Nu(x,y)$	Nusselt number = $h(x,y)d/k$
Nu_{ave}	Average Nusselt number
p	Pressure
q_w	Impinging surface local heat flux
T_{w}	Impinging surface wall temperature
T_{jet}	Jet inlet static temperature
V	Jet velocity at the exit of the piccolo tube
W	Jet-to-jet spanwise distance
x	x coordinate
y	y coordinate
ρ	Air density
μ	Air dynamic viscosity

1 Introduction

Turbulent impinging air jet has been encountered in many industrial and engineering applications, such as cooling of stock material during material-forming processes, glass tempering, cooling of electronic components, heating of optical surfaces for defogging, cooling of critical machinery structures, and many other industrial processes. Usually, impinging jets are often used when there is a strong demand for localized convective heat transfer rates [1–4].

Specifically, in the aviation industry, impingement jets have been used in turbine vanes cooling, developing vertical takeoff and landing aircraft, electronics packages cooling, cabin air-conditioning system and also in anti-icing thermal protection systems [5–9]. In typical engineering applications, such jets are usually under turbulent regime and arranged in banks to produce high transfer coefficients

Technical Editor: André Cavalieri.

✉ Cláudia R. Andrade
claudia@ia.br

[1] Aeronautical Engineering Division, Technological Institute of Aeronautics (ITA), Praça Marechal Eduardo Gomes, 50, Vila das Acácias, São José dos Campos, SP CEP 12228-900, Brazil

over an extended area. Heating or cooling of large-surface-area products is often carried out in device arrays of round or slot nozzles, through which air (or another gaseous medium) impinges vertically by enhancing the heat transfer mechanism.

It is well known that compared with classical convection cooling by confined flow parallel to the cooled surface, jet impingement produces much higher heat transfer coefficients once the attached boundary layers are much more thinner [10].

Furthermore, impingement flow devices allow for short flow paths on the surface and therefore relatively high heat transfer rate, mainly for aeronautical applications where weight and space are so restrictive conditions.

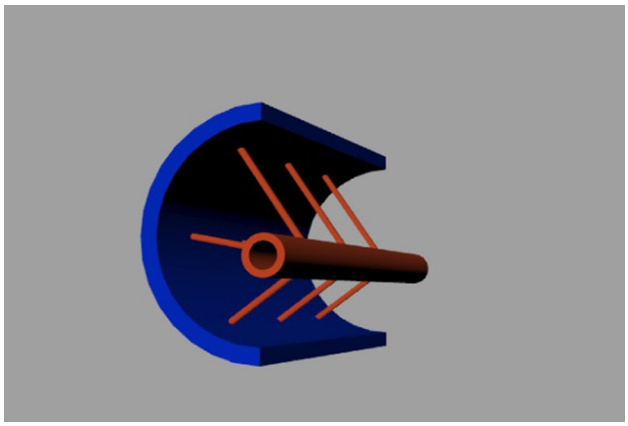

Fig. 1 Schematic representation of a hot-air anti-icing bleed system

1.1 Aircraft hot-air anti-icing systems

An accurate evaluation of the heat transfer rate in the hot-air anti-icing systems is of great interest to optimize both the anti-icing performance and the hot-air bleeding from the aircraft high-pressure compressor. The icing formation also has many effects on aircraft aerodynamics performance. Ice or snow on the wing can reduce the lift and increase the drag. According to a work published by the Civil Aviation Authority of New Zealand [11], research measurements taken on an aircraft with ice accretion disclosed a substantial increase of more than 60% in total drag and a loss of 17% in lift compared to a clean condition. These data were from a typical twin-engine commuter-type aircraft operation. If it is on leading edge, it may affect both of these to a greater degree. It may even change the point at which the airflow separates from the wing, altering the stall speed and stall characteristics of an airfoil.

Moreover, aircrafts should be equipped with two types of ice protection systems: deicing systems and anti-icing systems. The deicing systems work periodically, waiting that a small portion of ice attach on a surface before removing. Additionally, the anti-icing systems are designed not to allow any formation of ice, working continually at any indication of icing [12].

The most prevalent deicing and anti-icing technique is the use of hot bleed air from the high-pressure compressor of the engine due to the availability of bleed and the reliability of this technology [5]. The hot-air system is applied in the leading edges of the wing, tailplane and fin, empennages surfaces, radomes and jet engine air intakes. In general, the hot air is diverted from the source by interconnecting ductwork to the interior of the location to be anti-iced or deiced. For wings or engine inlets, the air is discharged from the ductwork into piccolo tubes or narrow-gap passages to transfer thermal energy to the aircraft skin along the chordwise direction. Figure 1 shows a typical hot-air anti-icing system. The rate of hot-air flow required for anti-icing or deicing is dependent on the source air temperature, heat losses through the ductwork, the geometry of the piccolo tube or narrow-gap passages and the parameters that affect ice accretion.

Design parameters such as the hole size and position or the specific mass flow could be carefully tuned from the knowledge of the temperature and flow fields [13].

However, the flow behavior within the slat is highly complex, as it spans both high-speed supersonic jets and a very-low-Mach-number core flow region. In addition, the heat transfer distribution along the inner side of the deicing surface is strongly influenced by the presence of large recirculating regions. Furthermore, three-dimensional effects can also be significant in the impingement jet-flow behavior as recently investigated in the literature [14]. Several studies have focused on the impingement jet-flow problem, considering both flat plates and concave impinging surfaces.

The effect of the jet orifice-to-plate spacing was experimentally studied in [15] at jet Reynolds number equal to 40,000. The authors tested three different jet arrays: single jet, 3 colinear jets and 7-jet array. For the single impinging jet case, a local minimum of Nusselt number was observed near the center of impingement for small jet-to-wall spacing ($z_n/d=2$). Their results also showed that the higher heat transfer coefficient values occurred for smaller spacing ($z_n/d=2$) in comparison with larger ones ($z_n/d=6$) when 7-jet and 3-jet arrays were taken into account.

The study of [16] investigated the effect of jet–jet spacing (c_n/d) and low nozzle–plate spacings (z_n/d) on the convective heat transfer in a flat-plate surface. Local and average Nusselt numbers were calculated for an array of axisymmetric air jets. The Reynolds number varied in the range of 3500–20,400. Their study revealed that when the nozzle-to-plate distance decreases to $z_n/d=1$, there are a significant enhancement of the average Nusselt number and a more uniform heat flux distribution over the impingement surface.

The effect of jet–jet spacing on the heat transfer for confined circular air jets impinging on a flat plate was investigated in [17]. The authors considered five jets in equilaterally staggered array and three different jet Reynolds numbers ($Re = 10{,}000$, 20,000 and 30,000). To evaluate the influence of jet–jet spacing (c_n/d), Reynolds number and nozzle–plate spacing (z_n/d) on the stagnation Nusselt number, a thermocouple technique was adopted to measure the local temperature on the impingement plate. From the experimental data obtained, it was concluded that the heat transfer of an impinging jet array is strongly affected by jet interference before impingement and/or jet source. According to the authors, the jet interference before impingement occurs in the case of a small jet–jet spacing due to the shear layer expansion. On the other hand, the jet source will form if the strength of the interaction of two adjacent wall jets is strong. Their results showed that both the effects, the jet interference before impingement and the jet source, deteriorate the overall heat transfer. Analyzing the results, the authors also identified two relative maxima of the Nusselt number at the stagnation point. These maxima occur due to the effects of the jet interference before impingement and the jet source.

An experimental study focused on the heat transfer optimization of a row of impinging jets on a flat plate was presented in [18]. They accurately evaluated the heat transfer characteristics, employing a heated-thin-foil technique coupled with infrared thermography. The results were analyzed in terms of local and average Nusselt numbers. To realize the optimization, the influence of the impingement distance, z_n/d, injection Reynolds number, Re, and spanwise distance between two holes of the row, c_n/d, where c_n is the spanwise distance between two holes, were taken into account. The measurements pointed out an optimum impingement distance (maximum heat transfer rates) within the range $z_n/d = 2$ and $z_n/d = 5$. Also, increasing Re and decreasing c_n/d tend to improve heat transfer rates.

Lee and Lee [19] experimentally investigated the turbulent heat transfer characteristics in a stagnation region of an axisymmetric submerged air jet impinging normal to a heated flat plate. The main objective of that study was to obtain a better understanding of impingement jet heat transfer characteristics near the stagnation region and provide benchmark heat transfer data. The experimental results showed that the stagnation Nusselt number can be correlated with the Reynolds number in which dependence is enhanced with increasing z_n/d. According to the authors, this is due to increase in the centerline turbulent intensity of the approaching jet. The results also showed that, for small nozzle-to-plate spacing of $z_n/d = 2$, the local heat transfer distributions have two distinct peaks. The authors explained that the first peak is due to the accelerated radial flow at the edge location of the nozzle and the second peak is due to the transition from laminar to a turbulent boundary layer. Another observation is that the locations of maxima shifted outward with increasing jet Reynolds number. For larger nozzle-to-plate spacings than $z_n/d > 6$, the results showed just one peak at the stagnation point and that the local heat transfer rate decreases monotonically with the radial distance.

Hannat and Morency [20] presented a complete modeling of the anti-icing/deicing system using a conjugate heat transfer approach. The turbulence effect was taken into account applying the k–ϵ shear stress transport model. Results computed for internal heat transfer coefficients were higher than the ones predicted by correlations commonly used in the literature [21].

The study of Bu et al. [22] presented experimental results for the jet impingement heat transfer concave surface. The authors showed that the heat transfer coefficient exhibited an approximate bell-shaped behavior, with the peak located close to the stagnation point. They investigated the jet Reynolds number effect on the impinging surface heat transfer, but the Mach number dependence was neglected.

Brevet et al. [23] experimentally studied a single-round jet impinging on a flat surface. They proposed a correlation as a function of the nozzle-to-plate spacing, Reynolds and Mach numbers, but the jet-to-jet spacing effect on the heat transfer characteristics was not treated in their study.

The experimental study of Park et al. [24] analyzed the separate effects of Reynolds and Mach numbers on flat-plate impingement jet-flow case. They showed that many heat transfer correlations currently in use are based on tests in which only the jet Reynolds number was varied. Hence, these data may be inaccurate for high Mach number conditions. However, the jet-to-jet spacing (W/d) effect on Nusselt number distribution was neglected.

Vinze et al. [25] conducted an experimental study considering the impingement jet on a flat-plate surface. They studied the influence of different parameters: (1) nozzle profiles (circular pipe, contoured nozzle and orifice), (2) Mach number, (3) Reynolds number and (4) nozzle-to-plate distance, but employing a single-jet configuration.

Limaye et al. [26] reported the influence of Mach number and Reynolds number on the heat transfer and recovery factor distributions considering a flat-plate impingement jet problem. They showed that as Reynolds number is increased, the heat transfer rate also enhanced at all radial distances from the stagnation point and at all nozzle-to-plate tested spacing. However, the jet-to-jet effect on Nusselt number distribution was not investigated.

Most of the cited works investigated the Nusselt number behavior considering the impingement jet problem on flat-plate surfaces. More recent studies have focused on the impingement jet on concave surfaces. The experimental study of Zhou et al. [27] investigated the curvature effects on the impingement jet flow on a curved surface as a function of the

Reynolds number, but the Mach number and jet-to-jet spacing (W/d) influences were not taken into account.

Yang et al. [28] conducted a combined experimental and computational study to investigate the heat transfer characteristics of impingement jets on the concave surface of the leading edge of a NACA0015 airfoil. Local and average Nusselt number results were presented as a function of the jet-to-jet spacing and the jet-to-impinging curved surface distance, but considering only sonic flow conditions ($Ma = 1$).

The study of Hadipour and Zargarabadi [29] analyzes the heat transfer characteristics of an impinging jet on a concave surface, whereas the jet-to-surface distances (H/d) parameter was tested, considering very small jet-to-impinging surface conditions which are not suitable to aeronautical current anti-icing applications.

At this context, the current study complements the Yang et al.'s [28] impingement jet-flow research, mainly for commercial aviation case where the Mach number is in the compressible subsonic range. The present work will be focused on the influence of the Mach number on the heat transfer mechanisms associated with the impingement jet on typical anti-icing protection systems since this parameter is extremely relevant for aeronautical application purposes. This paper is organized as follows: (1) problem description; (2) mathematical modeling and boundary conditions; (3) computational strategy; (4) results discussion and concluding remarks.

2 Problem description

The anti-icing system represents a penalty to the aircraft propulsion system because it utilizes hot bleed air to avoid wing ice formation [30]. Hence, it is very important to know the hot airflow requirements by identifying the impingement jet heat transfer mechanisms. Therefore, a simplified configuration composed by a single array of round hot-air jets impinging on a cylindrical curved surface will be considered. The jet emerges from a hole of constant diameter (d), located in the cylindrical surface axis. Numerical simulations are performed using the geometry and parameters illustrated in Fig. 2.

In order to reduce the computational efforts, symmetry properties can be employed resulting in a simplified computational domain, as shown in Fig. 3 for two different configurations.

3 Mathematical modeling

In the present study, RANS (Reynolds-averaged Navier–Stokes) equations for turbulent compressible fluid flow are numerically solved. Mass conservation,

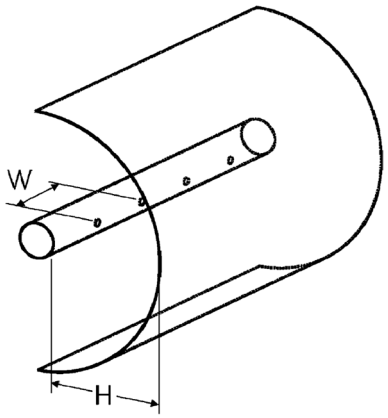

Fig. 2 Sketch of the impingement jet study: d = jet diameter; W = jet-to-jet spacing and H = jet-to-impinging surface distance

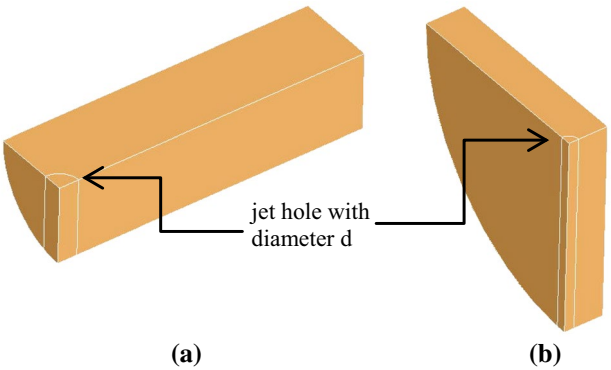

Fig. 3 Two different computational domains: **a** $W/d = 16$ and $H/d = 2$; **b** $W/d = 4$ and $H/d = 8$

momentum and energy equations in the conservative form [31] are given by:

$$\frac{\partial \rho}{\partial t} + \nabla \cdot (\rho \boldsymbol{U}) = 0 \tag{1}$$

$$\frac{\partial \rho \boldsymbol{U}}{\partial t} + \nabla \cdot (\rho \boldsymbol{U} \times \boldsymbol{U}) = -\nabla p + \nabla \cdot \left(\mu + \mu_t\right)\left(\nabla \boldsymbol{U} + (\nabla \boldsymbol{U})^T\right) \tag{2}$$

$$\frac{\partial (\rho h)}{\partial t} - \frac{\partial p}{\partial t} + \nabla \cdot (\rho \boldsymbol{U} h) = \nabla \cdot \left(k \nabla T + \frac{\mu_t}{Pr_t} \nabla h\right) + \nabla \cdot \left(\boldsymbol{U} \cdot \left(\tau - \rho \overline{u \times u}\right)\right) \tag{3}$$

where ρ is the fluid density; $\boldsymbol{U}$ is the mean velocity; p represents the pressure; μ and μ_t are the laminar and turbulent dynamic viscosities, respectively; h is specific enthalpy; k = fluid thermal conductivity; Pr_t = turbulent Prandtl number; and u is the velocity component in the x direction, respectively.

Turbulence effects are taken into account employing the k–ω–SST turbulence model [32], as follows:

$$\frac{\partial}{\partial t}(\rho k)+\frac{\partial}{\partial x_i}\left(\rho k u_j\right)=\frac{\partial}{\partial x_j}\left[\left(\mu+\frac{\mu_t}{\sigma_k}\right)\frac{\partial k}{\partial x_j}\right]+\widetilde{G_k}-Y_k+S_k \tag{4}$$

$$\frac{\partial}{\partial t}(\rho\omega)+\frac{\partial}{\partial x_i}\left(\rho\omega u_j\right)=\frac{\partial}{\partial x_j}\left[\left(\mu+\frac{\mu_t}{\sigma_\omega}\right)\frac{\partial\omega}{\partial x_j}\right]+\widetilde{G_\omega}-Y_\omega+D_\omega+S_\omega \tag{5}$$

The turbulent dynamic viscosity is computed from Eq. (6), as follows:

$$\mu_t=\frac{\rho k}{\omega}\frac{1}{\max\left[\frac{1}{\alpha_\infty^*},\frac{SF_2}{a_1\omega}\right]} \tag{6}$$

where

$$\sigma_k=\frac{1}{\frac{F_1}{\sigma_{k,1}}+\left(1-F_1\right)/\sigma_{k,2}};\sigma_\omega=\frac{1}{\frac{F_1}{\sigma_{\omega,1}}+\left(1-F_1\right)/\sigma_{\omega,2}};$$

$$\propto^*=\propto_\infty^*\left(\frac{\propto_0^*+Re_t/R_k}{1+Re_t/R_k}\right);Re_t=\frac{\rho k}{\mu\omega};\propto_0^*=\frac{\beta_i}{3};$$

$$F_1=\tanh\left(\phi_1^4\right);F_2=\tanh\left(\phi_2^2\right);$$

$$\phi_1=\min\left[\max\left(\frac{\sqrt{k}}{0.09\omega y},\frac{500\mu}{\rho y^2\omega}\right),\frac{4\rho k}{\sigma_{\omega,2}D_\omega^+y^2}\right];$$

$$\phi_2=\max\left(\frac{\sqrt{k}}{0.09\omega y},\frac{500\mu}{\rho y^2\omega}\right)$$

$$D_\omega^+=\max\left[2\rho\frac{1}{\sigma_{\omega,2}}\frac{1}{\omega}\frac{\partial k}{\partial x_j}\frac{\partial\omega}{\partial x_j},10^{-10}\right];$$

Table 1 presents a description of used symbols in the turbulence model equations.

The constant values of k–ω–SST model are: $\sigma_{k,1}=1.176$; $\sigma_{k,2}=1.176$; $\sigma_{\omega,1}=2.0$; $\sigma_{\omega,2}=1.168$; $a_1=0.31$; $\beta_{i,1}=0.075$; $\beta_{i,2}=0.0828$; $\alpha_\infty^*=1$; $R_k=6$; $\beta_i=0.072$. A more detailed and comprehensive review of available turbulence models can be found in [33].

4 Computational strategy

Numerical simulations have been carried out employing the CFD technique. A powerful tool to solve a great variety of engineering practical problems has been considered. Typical applications include chemical and manufacturing processes, electronic cooling devices, solar energy, wind turbines, automotive and aviation industries [34].

Table 1 Symbols of turbulence model equations

Symbol	Description
$\widetilde{G_k}$	Generation of turbulence kinetic energy due to the mean velocity gradients
$\widetilde{G_\omega}$	Represents the generation of ω
Y_k and Y_ω	Dissipation of k and ω due to turbulence
k	Turbulence kinetic energy
μ_t	Turbulent dynamic fluid viscosity
ω	Specific dissipation rate
σ_k and σ_ω	Turbulent Prandtl numbers for k and ε, respectively
y	Distance to the next surface
D_ω	Represents the cross-diffusion term
D_ω^+	Positive portion of the cross-diffusion term
S	Strain rate magnitude
F_1 and F_2	Blending functions
S_k and S_ω	User-defined source terms
i, j	Space components

In the current study, the subsonic compressible impingement jet flow over a concave surface problem was solved using a finite volume method code with a density-based approach [31]. The SIMPLE algorithm was utilized as a strategy for the velocity–pressure coupling with a segregated formulation. The numerical scheme was evaluated using second-order discretization for the advective terms and pressure. All simulations were carried out until the maximum residuals of the continuity, momentum and turbulent quantities reach a value of 10^{-5}.

4.1 Validation of the numerical procedure

Firstly, the procedure to obtain the numerical solution of the impingement jet on a concave surface was validated using the impingement jet on a flat-plate surface problem due to experimental data availability for comparison purposes [21]. Numerical results for this benchmark configuration were also presented in Fregeau et al. [5]. A polyhedral mesh with 577,006 elements (Fig. 4) was selected after a mesh sensitivity study (Table 3). A turbulence intensity of 5% and a turbulent-to-molecular viscosity ratio equal to 30 were set at the jet inlet surface.

The computational domain is represented by a quarter of the original geometry due to symmetry conditions. Numerical simulation was performed for the parameters set listed in Table 2. For Mach number equal to 0.4 and jet inlet static temperature of $T_{\text{jet}}=300$ K, the total temperature is $T_{\text{jet\_total}}=309.6$ K and the total pressure is

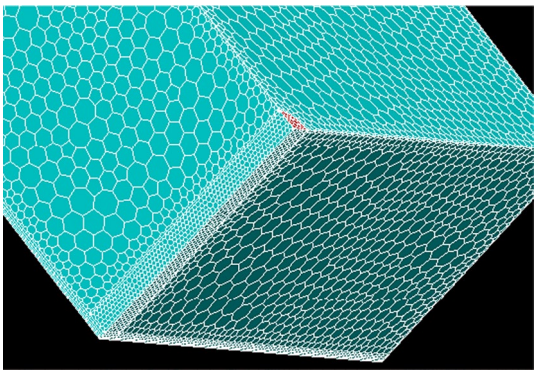

Fig. 4 Mesh view for impingement jet on a flat-plate surface

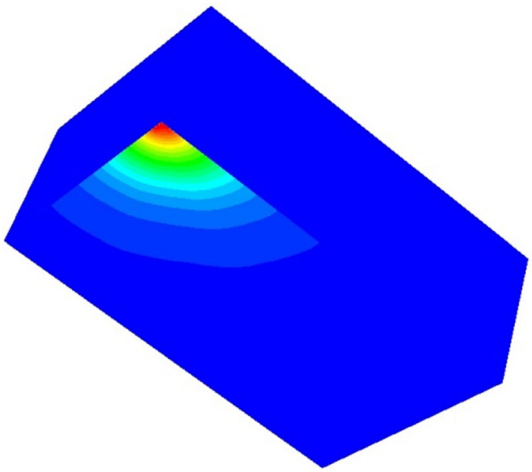

Fig. 5 Distribution of local Nusselt number along the impinging-wall surface

Table 2 Jet and operational conditions

Jet Mach number	0.4
Hole diameter d	6.35 mm
Jet height-to-diameter ratio, H/d	6
Jet spacing-to-diameter ratio, W/d	20
$\Delta T = T_{jet} - T_w$	20 K

11,809.6 Pa. The impinging surface is maintained with a constant wall temperature $T_w = 280$ K.

The heat transfer mechanism can be evaluated using the local Nusselt number as follows:

$$Nu(x,y) = \frac{h(x,y)\,d}{k} \tag{7}$$

where k is the fluid thermal conductivity and h is the local convection heat coefficient given by:

$$h(x,y) = \frac{q_w(x,y)}{(T_{jet\_total} - T_w)} \tag{8}$$

q_w is the impinging surface local heat flux and T_w is the impinging surface wall temperature. The average Nusselt number (Nu_{ave}) is determined using the following expression:

$$Nu_{ave} = \frac{1}{A}\int_A Nu(x,y)\,dA \tag{9}$$

where A is impingement surface area. As observed in Fig. 5, the local Nusselt number gradually drops from its maximum (close to the stagnation point) and decreases along the impinging-wall surface. Moreover, the strong curvature of the streamlines has a stabilizing effect on the flow structure, reducing the turbulence energy levels when the flow reaches the impingement area (wall-jet region).

The mesh sensitivity analysis is shown in Table 3 employing three different mesh densities. Observe that the average Nusselt number deviation between the intermediate and refined meshes is inferior to 1%.

Table 3 Mesh sensitivity study: impingement jet on a flat-plate surface

	Coarse	Intermediate	Refined
Elements number	412,308	577,006	726,240
Average Nusselt number	27.84	27.10	27.02

Table 4 Comparison of average Nusselt number for impingement jet on a flat-plate surface: validation case

	Gardon and Cobonpue [19]	Fregeau et al. [5]	Present study
Nu_{ave}	29.22	23.10	27.1
Diff.	0	20.9%	7%

Furthermore, a comparison of the average Nusselt number for impingement jet on a flat-plate surface is presented in Table 4. Note that the present study results are in good agreement with experimental data (deviation around 7%).

5 Results

In order to solve the impingement jet flow on a concave surface, the numerical simulations were performed with different jet hole diameters (1 mm $< d <$ 6.35 mm) to keep a constant Reynolds number condition, while the Mach number values are changed. The employed geometric parameters and Mach number are listed in Table 5, with a constant Reynolds number equal to 23,000.

Table 5 Tested Mach numbers and geometric parameters

Mach	0.2	0.4	0.6	0.8		
W/d	4	8	12	16		
H/d	2	3	4	6	8	10

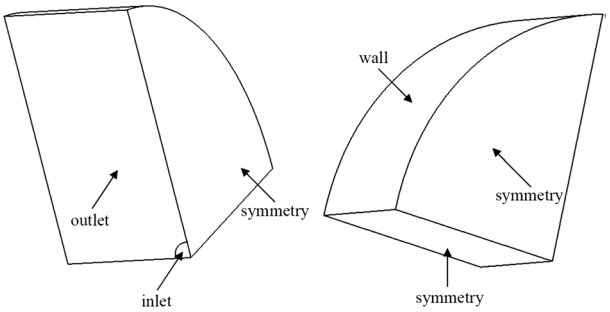

Fig. 6 Prescribed boundary conditions

The imposed boundary conditions are shown in Fig. 6. Moreover, symmetry condition was specified in the spanwise direction and through the middle of the piccolo jet. On the impinging concave wall, a no-slip constant temperature condition was imposed. A pressure boundary condition was set at the inlet and outlet boundaries.

Furthermore, a near-wall enhanced treatment combining a two-layer approach and conventional wall functions was utilized. In this method, the wall domain is subdivided into a viscosity-affected region and a fully turbulent region; thus, the enhanced wall functions act by smoothly blending an enhanced turbulent wall law with the laminar wall law. Besides, the wall *Y* plus value should be ~ 1 to ensure we are well capturing the laminar sub-layer adjacent to the surface concave wall.

Usually, the local Nusselt number distribution can be expressed in function of the geometric parameters and Mach number as:

$$Nu(x,y) = \frac{h(x,y)\,d}{k} = f\left(\frac{x}{d}, \frac{y}{d}, \frac{W}{d}, \frac{H}{d}, Ma\right) \quad (10)$$

where the local convection heat coefficient, *h(x,y)*, is determined using Eq. (8).

Figures 7 and 8 present the local Nusselt number distribution along the concave surface radial direction for two different jet-to-impinging surface distances $H/d = 2$ and $H/d = 8$, respectively. It can be observed that the maximum local Nusselt number occurs at the stagnation point and decreases in the downstream region from the jet centerline. The stagnation region is characterized by a change in the initial purely axial jet-flow behavior into a radial distribution. Consequently, this region generates a favorable pressure gradient that causes local flow acceleration, acquiring a wall-jet behavior further downstream. Moreover, the local Nusselt number values increase as a function of the *Ma* number. Hence, the stagnation *Nu* number value at $Ma = 0.8$ is approximately twice higher than $Ma = 0.2$ for both presented *H/d* values.

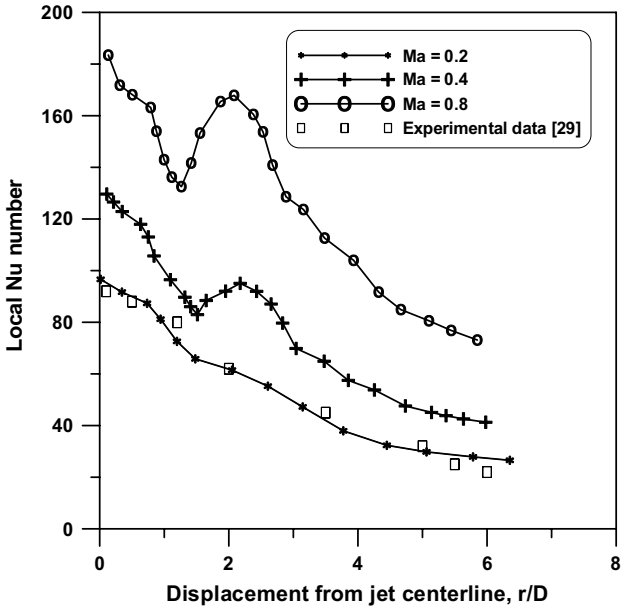

Fig. 7 Local Nusselt number distribution for $H/d = 2$ and $W/d = 12$

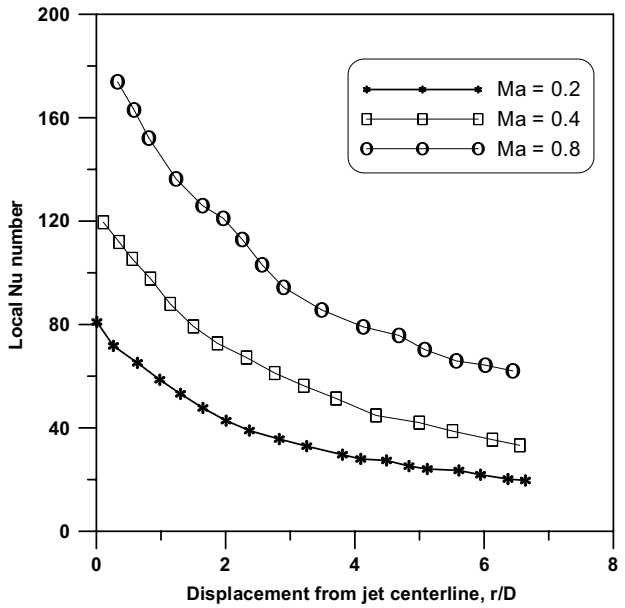

Fig. 8 Local Nusselt number distribution for $H/d = 8$ and $W/d = 12$

The local Nusselt number behavior is strongly dependent on the jet-to-impinging surface distance. For $H/d = 2$ (Fig. 7), the profile exhibits a first peak close to the stagnation zone as well as a secondary peak appears around $r/D = 2$. Then, the thickness of the viscous and thermal boundary layers increases, while the local Nusselt number gradually decreases as the jet spreads along the concave impinging wall. According to the literature [35], the Nusselt secondary peak e is linked to the near-wall flow dynamics and it appears at $H/d < 4$. In this condition, when the jet discharge is close to the impinging-wall surface, there is insufficient distance for significant mixing to occur with the surrounding fluid. Therefore, the thermal boundary layer stays confined to the thickness of the viscous sub-layer. Thus, high near-wall shear strains starts to develop which generate high turbulence levels and consequently a heat transfer rate enhancement.

On the other hand, Fig. 8 shows the local Nusselt number distribution for $H/d = 8$. In this case, there is only one maximum value close to the stagnation region. Then, the heat transfer mechanism intensity drops, and the local Nu number decreases as the jet spreads along the concave surface wall.

For aeronautical design purposes, the average Nusselt number is more relevant than the local value. This occurs because the hot bleed mass airflow rate should be determined based on Nusselt average values. Therefore, the average Nusselt number can be calculated as:

$$Nu_{\text{ave}} = \frac{h_{\text{ave}}\, d}{k} = g\left(\frac{W}{d}, \frac{H}{d}, Ma\right) \tag{11}$$

Table 6 exhibits the average Nusselt number (Eq. 11) results as a function of the mesh refinement at $Ma = 0.4$ and $W/d = 12$. As the jet-to-impinging surface distance (H/d) increases, a more refined mesh has been required to well capture the flow pattern both near and outside of the stagnation region (along the impinging curved wall). Furthermore, the average Nusselt number results are strongly dependent on the jet-to-impinging surface. At $H/d = 2$, the heat transfer mechanism is intense since the impinging surface is near the jet discharge, within its potential core region.

A similar study was also performed varying the jet-to-jet spacing (W/d). In these two tested parameters, the average Nusselt number calculated employing the intermediate and refined meshes did not change within 5%. Consequently, the intermediate mesh (see Fig. 9) was chosen due to computational effort saving.

Figure 10 shows static temperature contours with inlet Mach number equal to 0.4. Stagnation zone along the impinging wall reaches the high-temperature levels showing a great non-uniformity of the heat transfer mechanism. This behavior provides support to understanding the intense local Nusselt number variations presented in Fig. 7.

Table 6 Mesh sensitivity study: average Nusselt number results

$Ma = 0.4$ and $W/d = 12$			
H/d (mm)	Coarse	Intermediate	Refined
2	261,251	402,506	704,252
	67.81	66.48	66.42
6	222,136	423,034	736,114
	24.16	23.92	23.75
10	242,785	447,612	758,456
	15.12	14.76	14.64

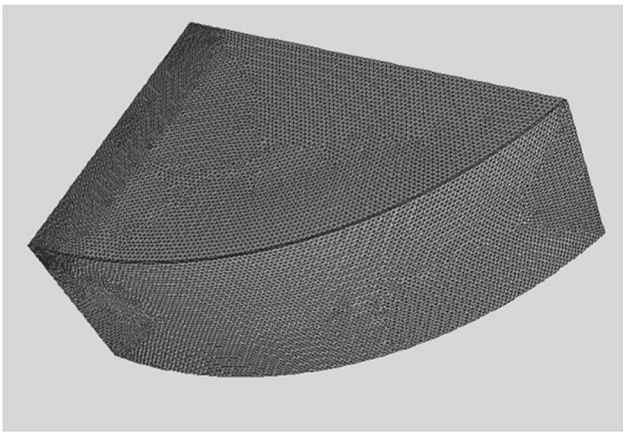

Fig. 9 Mesh view for impingement jet on a concave surface

Contours of Mach number for $H/d = 10$ and $W/d = 16$ are plotted in Fig. 11. It can be observed that the impinging surface is now positioned outside of the jet potential core, so the jet flow experiences an intense exchange of momentum with the surrounding air, reducing the impinging-wall heating. This behavior was also reported by [36] at high jet-to-surface distances ($H/d > 6$).

Contours of static temperature are presented in Fig. 12. As expected, maximum temperature values occur close to the stagnation point of the impinging wall, which leads to high local Nusselt number values (Eq. 10). When the hot-air jet impinges on the concave surface, the flow acquires a wall-jet pattern as it radially moves outward, reducing the heat transfer rate along the impinging surface curvature.

The analysis of Fig. 12 also shows a great non-uniformity in the temperature field leading to local variations of the heat transfer rate. Consequently, the average Nusselt number data are more advantageous than the local Nusselt number ones due to its less sensitive to spatial variations and thus much more reliable for engineering design purposes.

The effect of the jet-to-jet spacing (W/d) on the computed average Nusselt number (Eq. 11) for different impinging surface distances (H/d) is presented in Fig. 13 at Mach number equal to 0.4. These results show that the heat transfer rate

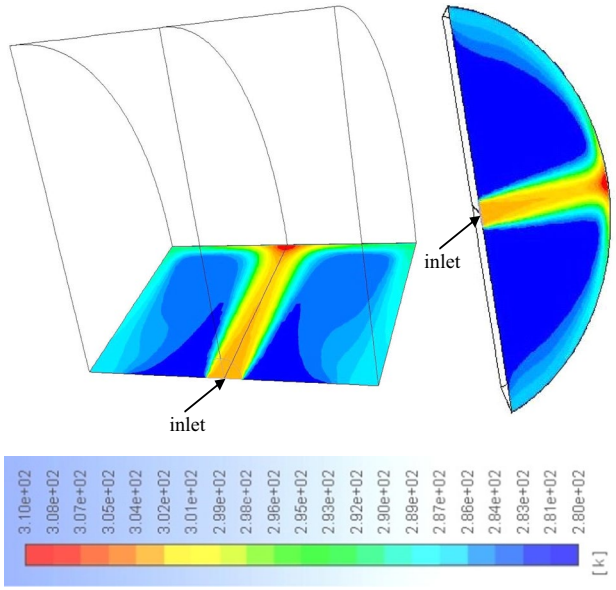

Fig. 10 Static temperature contours for $H/d=2$ and $W/d=8$ with inlet Mach number = 0.4 and $d=6$ mm

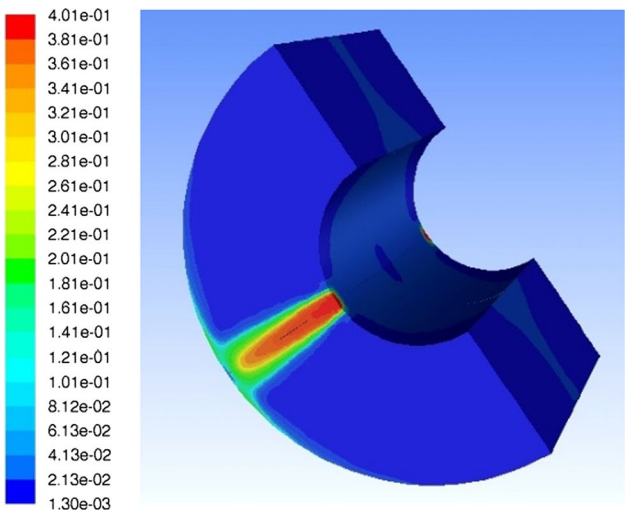

Fig. 11 Mach number contours for $H/d=2$ and $W/d=4$ with inlet Mach number = 0.4

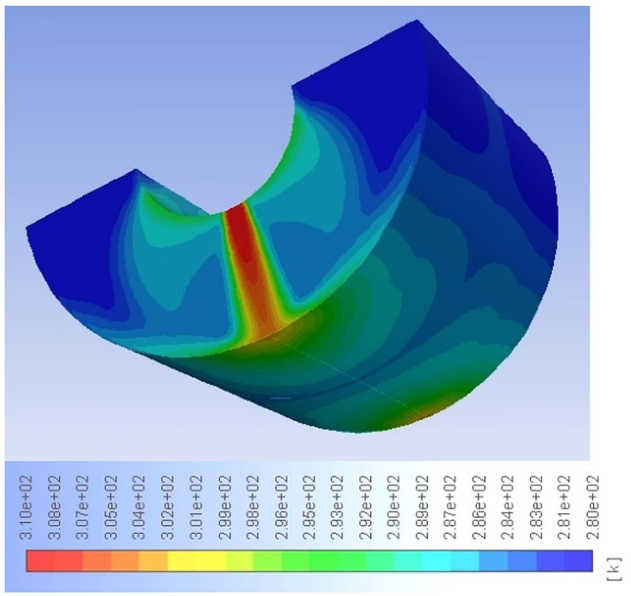

Fig. 12 Static temperature contours for $H/d=2$ and $W/d=4$ with inlet jet Mach number = 0.4

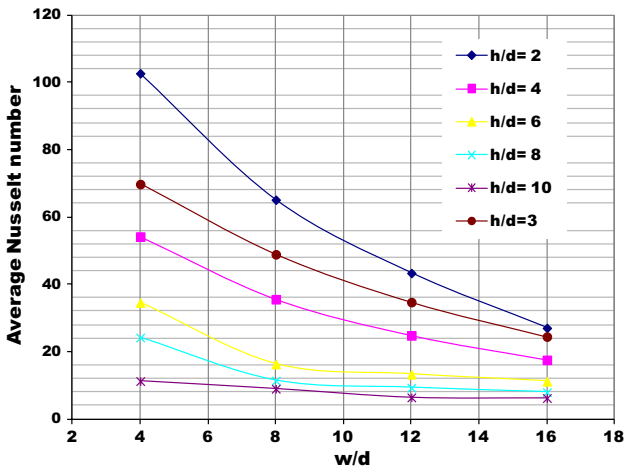

Fig. 13 Average Nusselt number as a function of the jet-to-jet spacing (W/d) at $Ma=0.4$ for different jet-to-impinging surface distances (H/d)

decays as W/d and H/d increase, but the impinging surface distance has a more pronounced effect on the average Nusselt number values decay in comparison with jet-to-jet spacing.

A similar behavior is also observed in the average Nusselt number distribution at Mach number equal to 0.8 (Fig. 14). The jet-to-jet spacing (W/d) influence on the average Nusselt number is weaker, mainly for $H/d>6$. At lower H/d conditions, i.e., lower jet-to-impinging surface distances, the temperature field exhibits a more efficient heating process inside the domain, resulting in greater Nu values, as presented in correlated literature studies [37]. This behavior is also linked with the displacement of the impingement region. Another literature experimental work [38] showed that the displacement of the impingement region was correlated to the fluid velocity when the impingement surface was near the nozzle ($H/d\sim2.5$) and independent of the fluid velocity when the surface was farthest from the nozzle ($H/d\sim8.5$).

On the other hand, the heat transfer rate is intensified as the Mach number elevates. For example, at $Ma=0.4$,

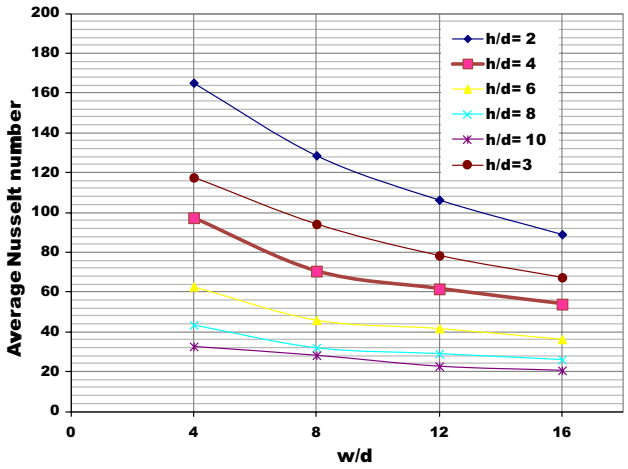

Fig. 14 Average Nusselt number as a function of the jet-to-jet spacing (W/d) at $Ma = 0.8$ for different jet-to-impinging surface distances (H/d)

$W/d = 4$ and $H/d = 3$, the average Nusselt number is ~ 70 (Fig. 13). This value reaches ~ 120 at $Ma = 0.8$, justifying an investigation about the Mach number effect on the anti-icing system employing concave impinging surfaces.

Table 7 shows average Nusselt number of numerical and correlation results, keeping the same Reynolds number in order to separately evaluate the Mach number effect. A comparison with the available literature value is also presented, for the jet-to-surface distance $H/d = 2$.

A good agreement with Hadipour and Zargarabadi's [29] result at $Re = 23{,}000$ (corresponding approximately to $Ma = 0.2$) can be observed. However, at higher Mach number values, the present results show that heat transfer rate is intensified due to compressibility effects action, but this parameter was not changed in Ref. [29] to allow comparison at $Ma > 2$.

Table 7 Average Nusselt number results at $Re = 23{,}000$

		$H/d = 2$ and $W/d = 4$
Hadipour and Zargarabadi [29] (no Mach number variation)		99.16
Present study: numerical results	$Ma = 0.2$	97.66
	$Ma = 0.4$	110.67
	$Ma = 0.6$	135.92
	$Ma = 0.8$	164.83
Present study: correlation results	$Ma = 0.2$	96.81
	$Ma = 0.4$	124.18
	$Ma = 0.6$	147.24
	$Ma = 0.8$	166.15

As pointed out by Brevet et al. [23], the Mach number has a relevant impact on the heat transfer enhancement along the impinging surface, and this parameter cannot be neglected.

Current study results allowed, concluding that as the Mach number increases, the average Nusselt number also elevates acquiring a power-law dependence ($Nu\ \alpha\ Ma^{0.42}$), as shown in Fig. 15. Two configurations for the jet-to-surface spacing (H/d) and jet-to-jet distance (W/d) are plotted.

Based on the curve fitting over 96 tested cases (see Table 5), it is possible to propose a correlation to evaluate the average Nusselt number for the hot-air impingement jets on concave surface, taking into account the Mach number as well as the geometric parameters:

$$Nu_{\text{ave}} = A\,(Ma)^{M}\left(\frac{W}{d}\right)^{N}\left(\frac{H}{d}\right)^{P} \tag{12}$$

where $A = 434.56$; $M = 0.42$; $N = -0.56$ and $P = -0.28$.

It is important to mention that Eq. 12 is valid in the following ranges: $0.2 \le Ma \le 0.8$; $2 \le H/d \le 10$, and $4 \le W/d \le 10$.

Figure 16 shows a comparison between numerical (Eq. 11) and proposed correlation results (Eq. 12) for the average Nusselt number obtained along the impinging concave surface wall (with $H/d = 2$ and $W/d = 4$). A good agreement level, with deviations inferior to 10%, can be observed. The correlation data also satisfactorily agree with the available literature result provided by Hadipour and Zargarabadi [29], as shown in Table 7 ($Ma = 0.2$).

6 Concluding remarks

This work studied the heat transfer mechanism in hot-air impingement jet on concave surfaces encountered in typical aircraft anti-icing systems. The jet-to-jet spanwise and jet-to-impinging surface distances were tested using different Mach number values. Results showed that the heat transfer

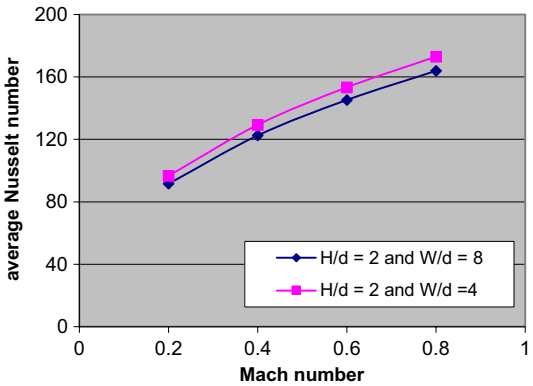

Fig. 15 Nusselt number as a function of the Mach number

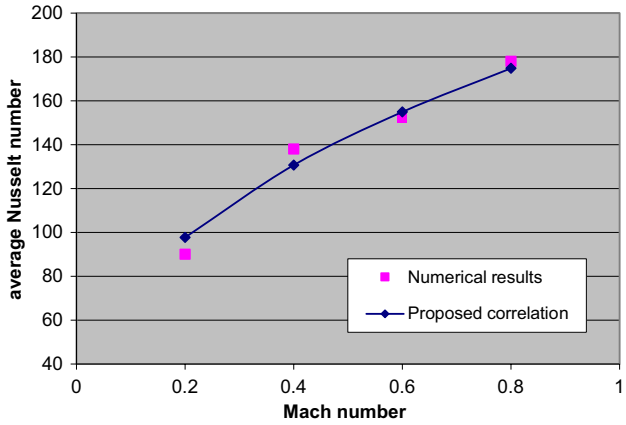

Fig. 16 Numerical data and proposed correlation values for the average Nusselt number

rate is intensified when the jet-to-impinging-wall distance is shorter, also reducing the jet-decay effect. Moreover, the Mach number has a relevant impact on the heat transfer enhancement in the impinging concave surface, and this parameter should not be neglected. A correlation has been proposed to evaluate the average Nusselt number taking into account the jet-to-jet spacing and the jet-to-impinging surface distance with good accuracy in the subsonic regime $0.2 \leq Ma \leq 0.8$.

Compliance with ethical standards

Conflict of interest The authors declare that they have no conflict of interest.

References

1. Oztekin E, Aydın O, Avcı M (2012) Hydrodynamics of a turbulent slot jet flow impinging, on a concave surface. Int Commun Heat Mass Transf 39:1631–1638
2. Zuckerman N, Lior N (2006) Jet impingement heat transfer: physics, correlations, and numerical modeling. Adv Heat Transf 39:565–631
3. Beitelmal H, Saad MA, Patel CD (2000) The effect of inclination on the heat transfer between a flat surface and impinging two-dimensional air jet. Int J Heat Flow 21:156–163
4. Chung YM, Luo KH, Sandham ND (2002) Numerical study of momentum and heat transfer in unsteady impinging jets. Heat Fluid Flow 23:592–600
5. Fregeau M, Saeed F, Paraschicoiu I (2005) Numerical heat transfer correlation for array of hot-air jets impinging on 3-dimensional concave surface. J Aircraft 42:665–670
6. Brown JM, Raghunathan S, Watterson JK, Linton AJ, Riordon D (2002) Heat transfer correlation for anti-icing systems. J Aircraft 39:65–70
7. Wright WB (2004) An evaluation of jet impingement heat transfer correlations for piccolo tube application. In: 42nd AIAA aerospace sciences meeting and exhibit, AIAA, pp 4153–4162
8. Ma H, Chen W, Zhang D (2012) Numerical investigation of engine inlet vane hot-air anti-icing system with surface air film. Int J Modern Phys Conf Ser 19:331–340
9. Castro TP, Andrade CR, Zaparoli EL (2014) Mach number effect on the heat transfer mechanism of aircraft anti-icing systems. Int Rev Mech Eng 8:547–554
10. Oztekin E, Aydın O, Avcı M (2013) Heat transfer in a turbulent slot jet flow impinging on concave surfaces. Int Commun Heat Mass Transf 44:77–82
11. Civil Aviation Authority (CAA) of New Zealand (2000) Aircraft icing handbook, p 108. https://www.caa.govt.nz/safety_info/GAPs/Aircraft_Icing_Handbook.pdf
12. Moir I, Seabridge A (2001) Aircraft systems: mechanical, electrical, and avionics, subsystems integration. AIAA education series. Professional Engineering Publishing, London
13. Ingole SB, Sundaram KK (2012) Review of experimental investigation in heat transfer for jet impingement cooling. Int Rev Mech Eng 6:346–356
14. Dewan A, Gupt DP, Sanghi S (2013) Enhancement of heat transfer through jet impingement by using detached ribs. Int Rev Mech Eng 7:308–317
15. Goldstein RJ, Timmers JF (1982) Visualization of heat transfer from arrays of impinging jets. Int J Heat Mass Transf 25:1857–1868
16. Huber AM, Viskanta R (1994) Effect of jet-jet spacing on convective heat transfer to confined, impinging arrays of axisymmetric air jets. Int J Heat Mass Transf 37:2859–2869
17. San JY, Lai MD (2001) Optimum jet-to-jet spacing of heat transfer for staggered arrays of impinging air jets. Int J Heat Mass Transf 44:3997–4007
18. Brevet P, Dejeu C, Dorignac E, Jolly M, Vullierme JJ (2002) Heat transfer to a row of impinging jets in consideration of optimization. Int J Heat Mass Transf 45:4191–4200
19. Lee J, Lee SJ (1999) Stagnation region heat transfer of a turbulent axisymmetric jet impingement. Exp Heat Transf 12:137–156
20. Hannat R, Morency F (2014) Numerical validation of conjugate heat transfer method for anti-/de-icing piccolo system. J Aircraft. https://doi.org/10.2514/1.c032078
21. Gardon R, Cobonpue J (1961) Heat transfer between a flat plate and jets of air impinging on it. Int Dev Heat Transf ASME, New York, pp 454–460. https://ntrs.nasa.gov/archive/nasa/casi.ntrs.nasa.gov/19730016200.pdf
22. Bu X, Peng L, Lin G, Bai L, Wen D (2016) Jet impingement heat transfer on a concave surface in a wing leading edge: experimental study and correlation development. Exp Thermal Fluid Sci 78:199–207
23. Brevet P, Dorignac E, Vullierme JJ (2001) Mach number effect on jet impingement heat transfer. Ann N Y Acad Sci 934:409–416
24. Park J, Goodro M, Ligrani P, Fox M, Moon HK (2006) Separate effects of Mach number and Reynolds number on jet array impingement heat transfer. J Turbomach 129(2):269–280
25. Vinze R, Chandel S, Limaye MD, Prabhu SV (2016) Effect of compressibility and nozzle configuration on heat transfer by impinging air jet over a smooth plate. Appl Thermal Eng 101:293–307
26. Limaye MD, Vedula RP, Prabhu SV (2010) Local heat transfer distribution on a flat plate impinged by a compressible round air jet. Int J Thermal Sci 49(11):2157–2168
27. Zhou Y, Lin G, Bu X, Bai L, Wen D (2017) Experimental study of curvature effects on jet impingement heat transfer on concave surfaces. Chin J Aeronaut 30(2):586–594

28. Yang B, Chang S, Wu H, Zhao Y, Leng M (2017) Experimental and numerical investigation of heat transfer in an array of impingement jets on a concave surface. Appl Thermal Eng 127:473–483
29. Hadipour A, Zargarabadi MR (2018) Heat transfer and flow characteristics of impinging jet on a concave surface at small nozzle to surface distances. Appl Thermal Eng 138:534–541
30. Lombardo D (1993) Advanced aircraft systems, 1st edn. McGraw-Hill Inc, New York, p 359
31. ANSYS/FLUENT Inc. (2010) User's guide Manual, 13.0 version
32. Versteeg HK, Malalasekera W (1995) An introduction to computational fluid dynamics—the finite method. Pearson, Prentice Hall
33. Argyropoulos CD, Markatos NC (2015) Recent advances on the numerical modelling of turbulent flows. Appl Math Model 39:693–732
34. Ströher GR, Zaparoli EL, Andrade CR (2013) Parabolic modeling of the pultrusion process with thermal property variation. Int Commun Heat Mass Transf 42:32–37
35. Aillaud P, Duchaine F, Gicquel LYM, Didorally S (2016) Secondary peak in the Nusselt number distribution of impinging jet flows: a phenomenological analysis. Phys Fluids 28:095110
36. Lee DH, Chung YS, Won SY (1999) The effect of concave surface curvature on heat transfer from a fully developed round impinging jet. Int J Heat Mass Transf 42:2489–2497
37. Ying Z, Guiping L, Xueqin B, Lizhan B, Dongsheng W (2017) Experimental study of curvature effects on jet impingement heat transfer on concave surfaces. Chin J Aeronaut 30(2):586–594
38. Frosell T, Fripp M, Gutmark E (2018) Dynamics of the impingement region of a circular turbulent jet. Exp Thermal Fluid Sci 91:399–409